REPORT

AIP/3 Experiment:
A Test of the Garand/Moeller Rain Classification Scheme

David W. Martin

NASA Grant NAG5-1586

A Tropical Rainfall Analysis Experiment for TRMM Using Ancillary Satellite Data

Verner E. Suomi
Principal Investigator

Space Science and Engineering Center
University of Wisconsin--Madison

1225 West Dayton Street
Madison, WI 53706

March 1995

AIP/3 Experiment:
A Test of the Garand/Moeller Rain Classification Scheme

SUMMARY

In this interim report we describe a test of the utility of Garand's cloud classification scheme for estimating rain. Garand's scheme employs pattern recognition to classify clouds viewed by the seventh Geostationary Operational Environmental Satellite at visible and at window infrared wavelengths. It operates on 100 km boxes within individual image pairs. We adapted the scheme to operate on visible/infrared image pairs and single infrared images from the Geostationary Meteorological Satellite. Borrowing sets of these images from the third Algorithm Intercomparison Project of the Global Precipitation Climatology Project, we applied the scheme to cases of rain falling over the equatorial western Pacific Ocean. Garand cloud classes were compared both with cloud classes and rain classes assigned manually using sequences of images rather than individual images.

The modified Garand scheme found much cloud and many cold tops in the sample, but not all classes. During the daytime cloud was bright as well as cold. Even by tropical standards the sample appeared to be wet. From a comparison of the visible/infrared assignments with the infrared-only assignments we infer that the infrared version of the Garand scheme weights cirrus at the expense of cumulus. It favors uni-layer cirrus classes over multi-layer cirrus classes. Probably because of these infrared-only weaknesses, the match of Garand classes to manual classes jumped from modest for the full set of classifications to good for the visible/infrared classifications. Together with a relatively small difference between full-set and visible/infrared classifications in the manual sample, this result suggests that Garand misses significant cloud information contained in the infrared images. Nevertheless, to the extent that the manual assignments reflect actual rain rates, even the infrared version of Garand provides information on rain.

The test suggests several courses. In the near term, we should explore the sensitivity of the scheme to cirrus clouds and compare the Garand classes with radar rain rates. We also should expand the study to a more representative sample of Algorithm Intercomparison scenes. If the radar comparisons conform to the manual comparisons, in the broader context of the Tropical Rainfall Measuring Mission, we should strip the superfluous classes from Garand, combine any redundant classes and retrain Garand for the tropics. We also should look into the possibility of extending G/M to include scale in space and change in time. As the culminating step in this sequence, we should convert Garand from a cloud classification scheme into a rain classification scheme.

We test the feasibility of estimating rainfall in the western equatorial Pacific Ocean using the scheme developed by Garand (1988). This scheme employs pattern recognition to classify clouds in a visible/infrared geostationary-satellite image of a mid-latitude ocean. Garand implemented it on a University of Wisconsin computer, the Man-computer Interactive Data Access System (McIDAS).

Garand (1989) demonstrated that the scheme extracts information on probability of rain as well as cloud type. Four years ago we began to explore its potential for contributing estimates of rain to the Tropical Rainfall Measuring Mission (TRMM). This report describes one of a series of experiments we have conducted to assess the power of the Garand scheme to estimate rain rate over the tropical oceans.

Background

The Garand scheme

Garand's 1988 scheme assigned clouds to one of the twenty classes listed in Table 1. It operated on a Geostationary Operational Environmental Satellite (GOES) infrared image of 4 km resolution (at the subpoint of the satellite) and its visible "mate" of 2 km resolution. The scheme processed an image pair in chunks, each containing 32 lines and 32 elements of the infrared data and 64 lines and 64 elements of the visible data. Thus, a nominal box measured 128 km by 128 km. The scheme allowed the user to specify both a starting line and element and the dimensions of an array of boxes. It required the user to specify a file into which the scheme could write the results of its calculations. These results could include values for predictors--the features determining cloud class--as well as assignments of cloud classes. To account for solar illumination angle, through a calibration of the visible channel the scheme increased visible digital counts to a condition of overhead sun.

As he restored Garand's code to McIDAS for TRMM, C. Moeller incorporated certain improvements. He enabled the code to accept image data of 4 km resolution in both channels, to run on infrared images only and to accept data from the fourth Japanese Geostationary Meteorological Satellite (GMS-4) as well as the GOES. The extension to GMS-4 required a calibration for the visible channel of that satellite. W. Rossow supplied that calibration, which draws on the International Satellite Cloud Climatology Project (ISSCP).

The extension of the scheme to infrared-only classification deserves comment. Moeller accomplished this extension by disabling the visible condition for cloud cover. In the absence of the visible condition the scheme calculates a threshold cloud temperature (T′) as

$$T' = SST - \delta T - 6.5K,$$

where SST is sea-surface temperature and δT is a correction for water-vapor absorption of longwave radiation upwelling from the surface. The constant term at the end of the equation assumes that cloud base lies 1 km above the sea surface in an atmosphere cooling upwards at a rate of 6.5 K km^{-1}. If the temperature of a pixel exceeds T′, the scheme assigns that pixel to the clear class (in Garand's nomenclature, class 1). Therefore, the calculation of cloud fraction depends on SST and δT.

Table 1. Garand Cloud Classes

Number	Name	Number	Name
1	clear	11	bright closed cells
2	stratus	12	nimbostratus
3	scattered cumulus	13	altocumulus
4	broken cumulus	14	altocumulus with cumulus
5	scattered stratocumulus	15	altocumulus with stratocumulus
6	broken to overcast stratocumulus	16	thin cirrus
7	cloud streets	17	multilayers with cirrus
8	bright rolls	18	multilayers with cumulonimbus
9	polygonal open cells	19	dense cirrostratus
10	strongly convective open cells	20	overcast cumulonimbus

The eastern Pacific test

Earlier we had run a test of the Garand/Moeller (G/M) code on GOES-West images of the eastern tropical Pacific (Suomi *et al.*, 1993). Lacking independent classifications of either cloud or rain rate, we verified the McIDAS (G/M) cloud classes against subjective cloud and rain classes. To assign a cloud or rain class, we could view up to three image pairs--each an hour apart--rather than the "target" image pair only. Animation helped especially in differentiating clouds by level and in isolating deep convection. Scenes were selected to span a range of cloud conditions. Rain rate was assigned to one of four categories: nil, light, moderate and heavy.

In the eastern Pacific test, G/M and subjective cloud classes agreed quite well. However, the test indicated that up to one-fifth of Garand's original classes (*e.g.*, nimbostratus) were not relevant to the equatorial maritime tropics. Further, G/M did not assign a few classes (*e.g.*, overcast cumulonimbus) which we expected and had assigned subjectively.

As expected, particular G/M cloud classes and groups of cloud classes tended to associate with particular rain classes. For example, "multi-layer cirrus" and "thick cirrus" classes of cloud associated with "moderate" and "heavy" classes of rain. The test supported our conjecture that Garand's scheme could aid TRMM and it suggested possibilities for improving it. But it could not speak for other parts of the tropical oceans nor could it provide a ground-based measurement of rain.

The third Algorithm Intercomparison Project

The third Algorithm Intercomparison Project (AIP/3; Arkin and Xie 1994) aims to test schemes for estimating equatorial rain rate over the oceans from observations of an operational meteorological satellite. AIP/3 piggybacks on the Coupled Ocean-Atmosphere Response

Experiment (COARE) of the Tropical Oceans Global Atmosphere (TOGA) project (Webster and Lukas 1992). COARE ran from 1 November 1992 through 28 February 1993. It featured calibrated Doppler radars, one on each of two ships positioned about 150 km apart on the second parallel south of the equator in the western Pacific Ocean. As in previous Algorithm Intercomparisons, AIP/3 participants agreed to certain conditions of location, duration, period, resolution, frequency, database and disclosure. The coordinators in turn offered each participant a database of satellite and other information. They withheld gauge and radar observations of rain until a participant submitted his or her estimate. The coordinator of AIP/3--the Research Centre of Australia's Commonwealth Bureau of Meteorology (BMRC)--is collating estimates, calculating certain measures of performance and distributing results to the participants. Late in March 1995 it will host a workshop for participants.

AIP/3 covers the patch of Pacific Ocean between 1°N and 4°S, 153°W and 158°W for the full period of COARE. It includes a 120 day sequence of GMS data. The sequence consists of 1320 slots for visible images and 2880 slots for infrared images. Not all slots contain images. Inadvertantly, a few slots contain duplicate images. Each image consists of 12,320 pixels (110 lines, each of 112 elements). A pixel measures 5 km by 5 km. If visible-wavelength, the pixel gets one of 64 levels of intensity, or gray; if infrared-wavelength, one of 256 levels. In a few infrared images pixels corresponding to temperatures colder than -80°C are set to a count of 255. In a few images transmissions garbled part or all of a scan line.

Anticipating the AIP/3 workshop, a BMRC scientist, E. Ebert, selected fifteen case studies. These are listed in Appendix A. Ebert's choices depended both on "something" of interest in observations from moored optical rain gauges and coinciding observations from GMS, the Special Sensor Microwave Imager (SSM/I) and the Advanced Very High Resolution Radiometer (AVHRR).

As a participant in AIP/3, SSEC intended to submit a set of G/M estimates. Because of the time required to run G/M on the mainframe McIDAS, this proved to be impractical. Instead, for the AIP we submitted four estimates based on simple infrared schemes. After submitting our AIP/3 rain estimates, for our own purposes we applied G/M to each of the fifteen cases. This application became the "AIP/3 Experiment."

Design

The AIP/3 Experiment aims to test three propositions.

- G/M does not quite fit the tropics.
- In its infrared version, G/M barely fits the tropics.
- Nevertheless, G/M can compete with infrared techniques like the GOES Precipitation Index (Arkin and Meisner, 1987).

Because of a delay in the release of the COARE radar rainfall data, by following the procedure devised for the eastern Pacific test, for the AIP/3 Experiment the author subjectively estimated rain rate. Nominally, class zero encompasses rain rates up to 0.05 mm h^{-1}; class 1, rain rates from 0.05 up to 1.0; class two, rain rates from 1.0 up to 10; and class three, rain rates of 10 and up. All rain in the present report references these subjective estimates.

Definitions

A *case* refers to one of the Ebert selections. Rather than being strictly limited to the period Ebert specified, it spans the seven hours centered on an Ebert case. We combined two closely spaced cases; thus, the AIP/3 Experiment consists of fourteen rather than fifteen cases. These fourteen cases are numbered chronologically. In the context of these cases a *slot* refers to the place of one of the infrared or visible/infrared images in the GMS sequence comprising a case. Nominally, slots fall at hourly intervals (on the half-hour) and a case consists of seven slots. (The combined case consists of nine slots.) For the ordinary cases, images in the second, fourth and sixth slots were processed: these are the *base images*. For the combined case, the image in the eighth slot was processed as well. First, third, fifth and seventh slots contain the *reference images*. Thus, nominally, the interval between base images is two hours. Base images are numbered consecutively. There are 43. For the AIP/3 Experiment the *box* over which G/M classifies clouds consists of 32 lines and 32 elements. It measures 160 km by 160 km. Boxes are arrayed in three contiguous rows and three contiguous columns and numbered (1, 2, 3, ... 9) by row and by column from top left to bottom right. The upper-left (northwest) corner of the first box in the array lies at 00°42′03″N, 153°11′27″W. Finally, a *scene* consists of one of the 382 boxes which remained after base images had been checked for false infrared counts and garbled lines. (These checks resulted in the rejection of five boxes.) Scenes are numbered consecutively by box within a base image, by base image within a case and by case.

Case by case, the author also checked base images for duplication, for continuity, for registration of visible and infrared channels (of an image pair) and for registration of the infrared images (reference as well as base) in the sequence comprising a case. One duplicate image was found and two images were out-of-sequence. All three images fell into reference slots. All visible/infrared image pairs registered to within one pixel. In three cases (4, 9 and 10) we corrected a misregistered sequence by shifting one of the images or image pairs in line or element or both.

Procedure

We processed the GMS images on two linked computers, a PS-2 work station and an IBM 4381 T92 mainframe computer. Both run McIDAS programs, but only on the mainframe computer can run G/M. We set SST to 302.2°K (29°C) and δT to 6K. Details of the processing are recorded in a script which the author will provide on request. Here only the main steps are listed.

> For the first case, create a mainframe file to receive the output (both features and cloud classes) from G/M. Copy the GMS images for all slots from diskette to the mainframe. Display the images on the work station. Edit the images and flag any bad scenes. For base images, with the graphics off, calculate features and classes. Referring to reference images as needed, assign cloud and rain classes. Copy G/M output to diskette. Recreate the mainframe output file and go on to the second case. Continue until all cases have been processed.

First-, second- and third-choice G/M cloud classes were copied into a spreadsheet. Certain features were copied as well: a measure of minimum cloud-top temperature (in Garand's code,

TTOP), fractional cloud cover (CFFX) and cloud average reflectance (CREF). Manual cloud classes and rain classes were entered into the same spreadsheet.

Results

The cases cluster around dawn (Figure 1), when large, cold clusters tend to be most frequent (Mapes and Houze 1993). The distribution of minimum cloud top temperature (Figure 2) peaks at relatively cold values (186 to 190°K).

Figure 3 raises suspicions about the calculation of cloud fraction. Even for a set of wet cases from a strongly convective area of the earth, the spike in frequency for cloud fraction upwards of 0.95 seems excessive. Indeed, as is shown in Appendix B, in infrared-only mode the GMS version of G/M always calculates a cloud fraction in excess of 0.95. This preference for high values of fractional cloud cover may reflect our choice for the atmospheric correction, which could be too small.

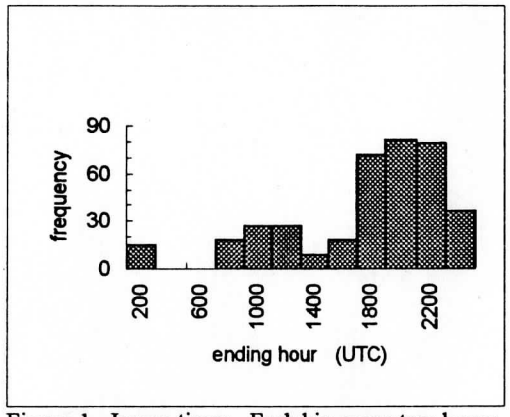

Figure 1. Image times. Each bin spans two hours. To convert to local time, subtract 10 h.

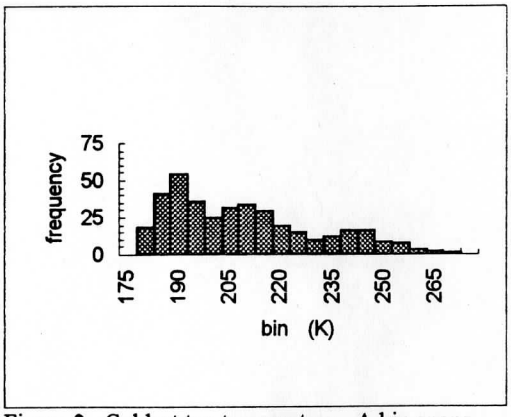

Figure 2. Coldest top temperature. A bin spans the five-degree interval ending at the indicated value. Thus, in 19 boxes (out of 382) the coldest top temperature fell in the interval from 175°K through 180°K.

Reflectance averaged over cloudy pixels (Figure 4) also proves to be high, perhaps to the point of casting doubt on the ISSCP calibration of the visible channel on GMS-4. Manually-assigned rain rates (Figure 5) reflect both these cloud distributions and very recent measurements of rain within and near the COARE domain (*e.g.*, Gage *et al.* 1994). Apparently, rain dominated most of the cases.

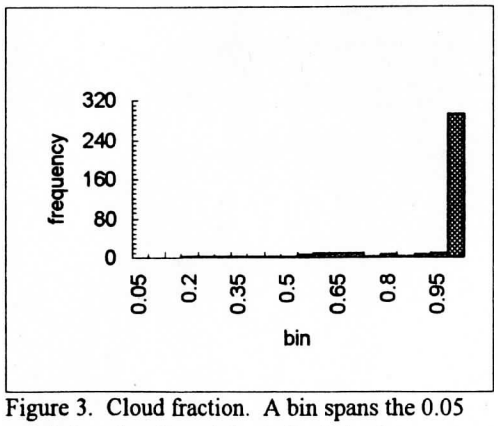

Figure 3. Cloud fraction. A bin spans the 0.05 unit interval ending at the indicated value.

The features (coldest cloud-top temperature, cloud fraction and cloud reflectivity; Appendix B) relate to one another as one might expect (*e.g.*, see Garand 1989). As top temperature increases, both cloud fraction and cloud reflectivity decrease. Cloud fraction increases with cloud reflectance. Reflectance correlates strongly with top temperature and cloud fraction (correlation coefficients of 0.60 and 0.58, respectively). For the bispectral set top temperature also correlates strongly with cloud fraction ($\rho = 0.70$). However, for the full set (not shown) it correlates only modestly with cloud fraction ($\rho = 0.37$).

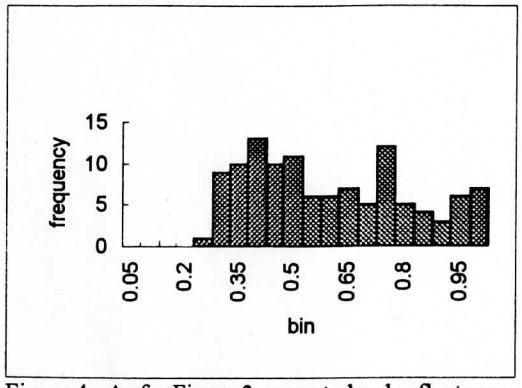

Figure 4. As for Figure 3, except cloud reflectance.

As shown by Figure 6, in the manual classification overcast cumulonimbus clouds (G/M 20) rule. To a degree this dominance reflects the author's inclination to give a cumulonimbus cloud precedence over all other cloud types. It also reflects his failure to note that Garand intended that class 18 include isolated cumulonimbus clouds. Classes of cirrus appear frequently. Classes characterized by multiple layers contribute significant numbers there (*e.g.*, G/M 17 and 18) and in the middle-cloud range as well (G/M 15). As with G/M, there are no occurrences of clear or nimbostratus (G/M 1 or 12), none of open cumulus cells (G/M 9 and 10) and only one of stratocumulus (G/M 5 and 6).

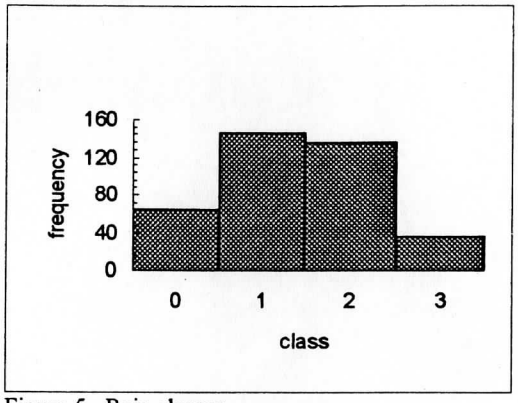

Figure 5. Rain classes.

As might be expected from the distributions of top temperature and cloud cover, G/M finds this set of scenes to be dominated by cirrus (Figure 7a). For the most part it splits the cirrus between thin (G/M 16) and thick/overcast (G/M 19) classes. G/M finds no occurrences of clear boxes. Neither does it find occurrences of nimbostratus or (except for cumulonimbus) of deeper cumulus. For the most part, in second-guessing itself, G/M simply rearranges frequencies in the cirrus classes (Figure 7b).). Manual classes correlate about equally well with machine first-choice and machine second-choice classes. At 0.32 and 0.34, both are disappointingly low.

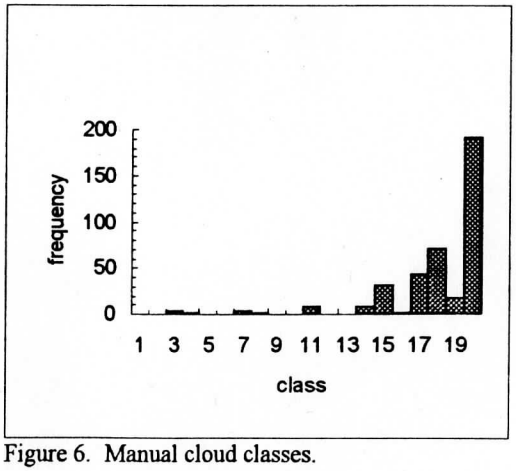

Figure 6. Manual cloud classes.

The effect of the visible channel is explored in comparisons of coldest cloud top temperature, cloud fraction and cloud reflectance for bispectral scenes and all scenes. As shown in Appendix C, the bispectral scenes are not as cold, not as cloudy and not as wet as the full set of scenes. Figure C.2 implies a phenomenal increase in nighttime cloud fraction. We attribute part of this increase to a flaw which makes G/M excessively sensitivity to cirrus clouds.

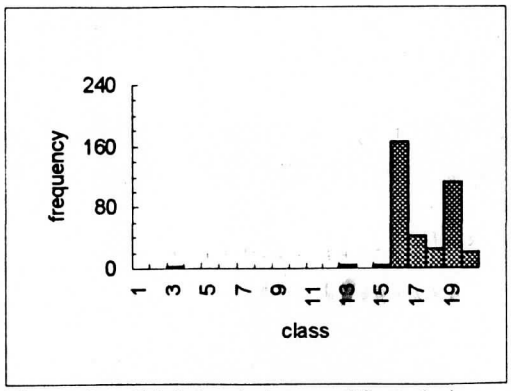

Figure 7a. G/M cloud classes of first choice.

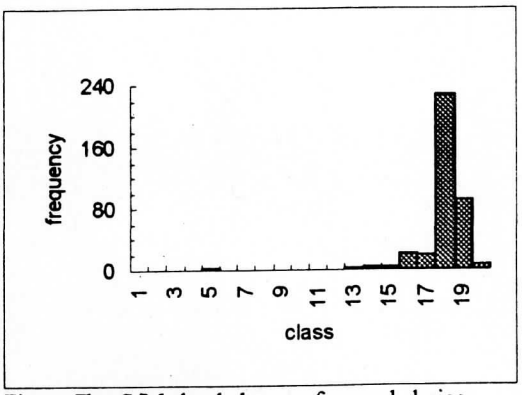

Figure 7b. G/M cloud classes of second choice.

The manual classification for bispectral images (Figure 8) differs from the full classification only in detail. However, G/M reverses relative frequencies in thin-cirrus and multilayer-cirrus classes (G/M 16 and 17), with bispectral classification favoring multilayer cirrus (Figure 9). For the bispectral images it also reverses frequencies in the multilayer-broken-cirrus, overcast-cirrus and cumulonimbus classes (G/M 18, 19 and 20), with the first and third gaining at the expense of the second. Thus, in spite of the author's inclination to assign scenes containing any cumulonimbus clouds to G/M 20, for the bispectral set of images the correlation of manual class to machine class improves to 0.49.

Predictably, in the full set of manual assignments every heavy-rain class contains cumulonimbus clouds (G/M 2 0; Figure 10). Each of the thin-cirrus and shallow-cumulus classes falls in either the nil- or light-rain classes. Broken- and solid-thick cirrus classes fall mainly in the light- and moderate-rain classes.

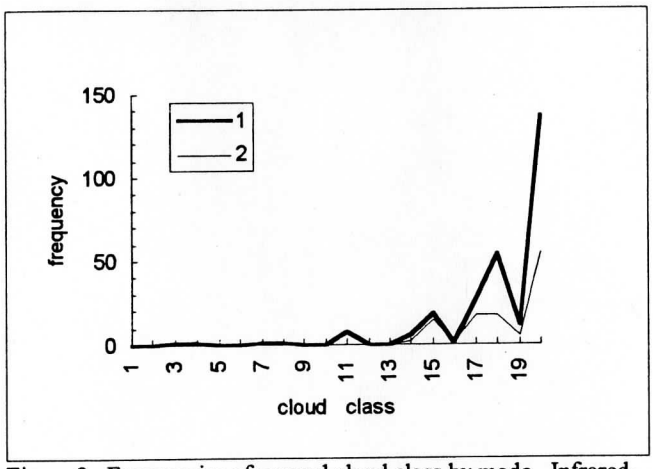

Figure 8. Frequencies of manual cloud class by mode. Infrared-only corresponds to 1; bispectral, to 2.

In the full set of G/M assignments thin cirrus (G/M 16) falls mainly outside the heavy rain class whereas solid cirrus (G/M 19) falls mainly outside the light class (Figure 11; also see Table 2). Cumulonimbus assignments favor the moderate rain class. Middle and low cloud assignments favor the nil and light classes. Within the multilayer category, assignments of cirrus of small thickness (G/M 17) lie on the light-rain side of assignments of cirrus of large thickness (G/M 18).

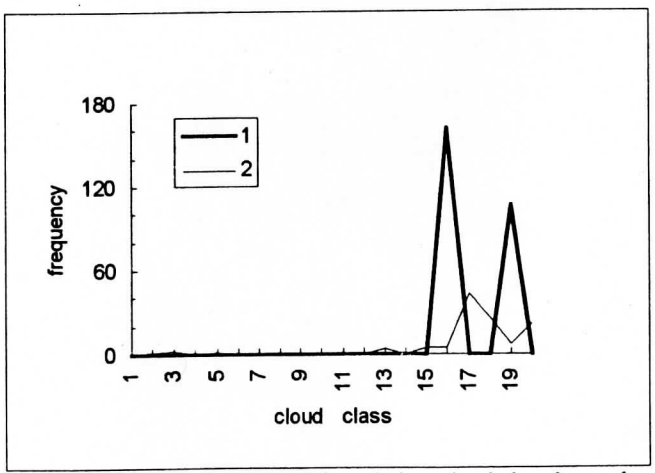

Figure 9. Frequencies of G/M (first choice) cloud class by mode.

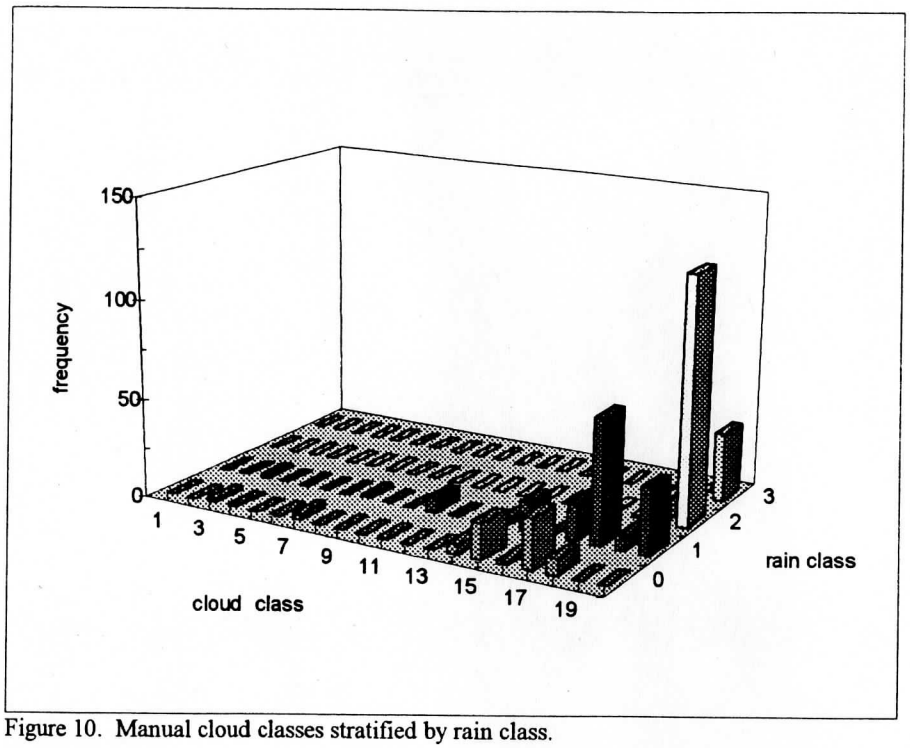

Figure 10. Manual cloud classes stratified by rain class.

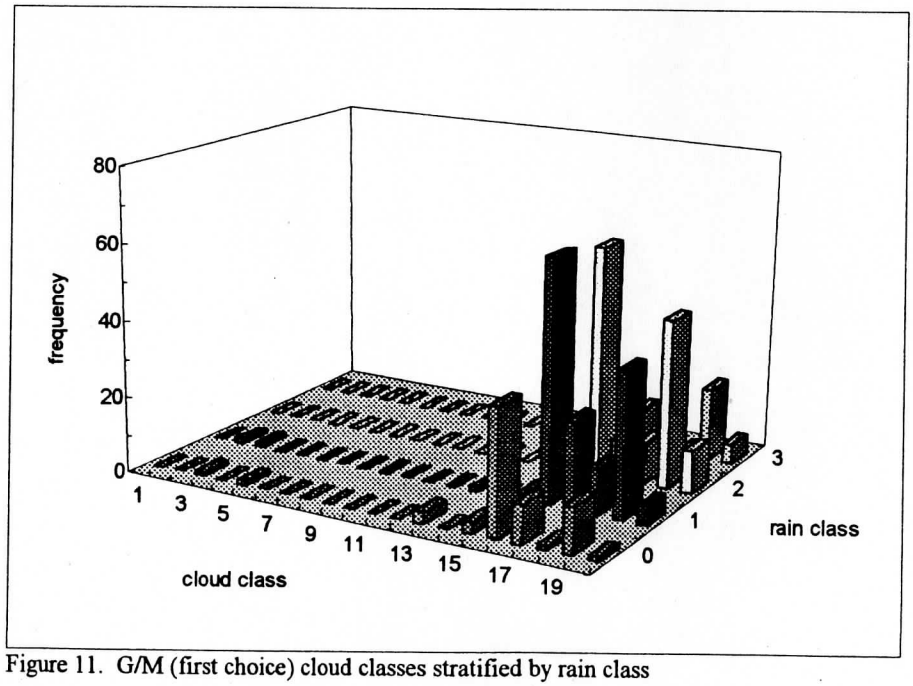

Figure 11. G/M (first choice) cloud classes stratified by rain class

Table 2. Frequencies of G/M cloud classes by rain class

Cloud Class	Rain Class				Cloud Class	Rain Class			
	0	1	2	3		0	1	2	3
1	0	0	0	0	11	0	0	0	0
2	0	1	0	0	12	0	0	0	0
3	1	1	0	0	13	3	1	0	0
4	0	0	0	0	14	0	0	0	0
5	1	0	0	0	15	3	2	0	0
6	0	0	0	0	16	33	63	60	10
7	0	0	0	0	17	10	23	10	0
8	0	0	0	0	18	1	12	11	1
9	0	0	0	0	19	12	38	44	19
10	0	0	0	0	20	1	5	11	5

Conclusion

We have described an experiment aimed at testing the proposition that a modified version of the Garand (1988) scheme for classifying clouds could be used to estimate rain rate over the equatorial western Pacific Ocean. The modified (G/M) scheme was applied to fourteen sets of GMS-4 infrared or visible/infrared images from the TOGA/COARE archive. Nominally, each image or image pair contained nine boxes. A box, the basic unit of classification, measured 160 km on each side. Independently, by examining a loop of images, we classified both clouds and rain rates for the same boxes. After we edited it for bad data, the sample contained 382 boxes. One-hundred sixteen of the 382 boxes referenced bispectral (visible and well as infrared) data.

Nighttime cloud cover probably was biased toward high values. Even during the daytime, G/M found much cloud and many cold tops in the sample. During the daytime, cloud was bright as well as cold. Inspection of the images indicated that even by tropical standards the sample was wet.

Comparing the bispectral subset of assignments with the full set, we infer that the infrared version of the Garand cloud classification scheme weights cirrus at the expense of cumulus. Within the cirrus classes, it favors single-layer (or overcast) over multi-layer. In short, the absence of the visible channel (a) tilts G/M toward cold clouds and (b) diminishes G/M's power to discriminate depth in cloud.

Probably because of these infrared-only weaknesses, the match of G/M classes to manual classes jumped from modest for the full set of classifications to good for the bispectral set of classifications. Manual assignments differed less from bispectral-only to full-set than did G/M assignments. This difference suggests that G/M misses significant cloud information contained in the infrared images. Plots of class frequency for the full set underscore a conclusion of the eastern Pacific study, that the present G/M scheme contains two or three superfluous classes.

During daylight as well as nighttime hours G/M favors cirriform over cumuliform clouds. Especially at night it sometimes fails to recognize a cumulonimbus cloud. Nevertheless, to the extent that the author's rain classes reflect actual rain rates, even the infrared-only version of G/M yields information on rain.

We recommend the following.

- Examine the sensitivity of infrared-only classification to the atmospheric correction.
- Extend the present study to include radar rain rates.
- Strip the classes which rarely or never occur over the tropical oceans, combine redundant classes and retrain G/M.
- Investigate the possibility of extending G/M to include scales in space and change in time.
- Building on G/M, devise a true *rain* classification scheme.

Acknowledgements

Barry Hinton offered assistance at numerous points in this study. Christopher Moeller fielded many questions about the Garand scheme. Louis Garand sanctioned our decision to resurrect his code.

References

Arkin, P. A., and B. N. Meisner, 1987: The relationship between large-scale convective rainfall and cold cloud over the Western Hemisphere during 1982-1984. *Mon. Wea. Rev.*, **115**, 51-74.

Arkin, P. A., and P. Xie, 1994: The Global Precipitation Climatology Project: First Algorithm Intercomparison Project. *Bull. Amer. Meteorol. Soc.*, **75**, 401-419.

Gage, K. S., C. R. Williams and W. L. Ecklund, 1994: UHF wind profilers: A new tool for diagnosing tropical convective cloud systems. *Bull. Amer. Meteorol. Soc.*, **75**, 2289-2294.

Garand, L., 1988: Automated recognition of oceanic cloud patterns. Part 1: Methodology and application to cloud climatology. *J. Climate*, **1**, 20-39.

---, 1989: Two automated methods to derive probability of precipitation fields over oceanic areas from satellite imagery. *J. Appl. Meteorol.*, **28**, 913-924.

Mapes, B. E., and R. A. Houze, Jr., 1993: Cloud clusters and superclusters over the oceanic warm pool. *Mon. Wea. Rev.*, **121**, 1398-1415.

Suomi, V. E., S. A. Ackerman, D. W. Martin and B. B. Hinton, 1993: *A Tropical Rainfall Analysis Experiment for TRMM Using Ancillary Satellite Data*. Space Science and Engineering Center of the University of Wisconsin-Madison, Madison, Wisconsin, 20 pp.

Webster, P. J., and R. Lukas, 1992: TOGA COARE: The Coupled Ocean-Atmosphere Response Experiment. *Bull. Amer. Meteorol. Soc.*, **73**, 1377-1416.

Appendices

A. AIP/3 Cases

YEAR	DATE	DAY		TIME	YEAR	DATE	DAY		TIME
		Julian	IOP*	UTC			Julian	IOP*	UTC
1992	6-Nov	311	6	631	1993	1-Feb	32	93	2045
		311	6	830			32	93	2223
		311	6	1023		2-Feb	33	94	31
	24-Nov	329	24	1531		6-Feb	37	98	830
		329	24	1730			37	98	1023
		329	24	1930			37	98	1231
	19-Dec	354	49	1623		8-Feb	39	100	1930
		354	49	1831			39	100	2131
		354	49	2131			39	100	2330
		354	49	2330		15-Feb	46	107	631
		356	51	2045			46	107	830
		356	51	2223			46	107	1023
	20-Dec	357	52	45		18-Feb	49	110	1730
	25-Dec	362	57	1623			49	110	1930
		362	57	1831			49	110	2131
		362	57	2030		20-Feb	51	112	1531
1993	2-Jan	2	63	1730			51	112	1730
		2	63	1945			51	112	1930
		2	63	2131		25-Feb	56	117	1743
	28-Jan	28	89	1623			56	117	1930
		28	89	1831			56	117	2131
		28	89	2030					

*Intensive Observing Period

B. Bispectral Scatterplots

Three figures show relationships between coldest cloud-top temperature, cloud fraction and cloud reflectivity for the bispectral scenes. Each figure consists of a scatterplot; a least-squares, linear regression line; and coefficients (including correlation) of the regression line.

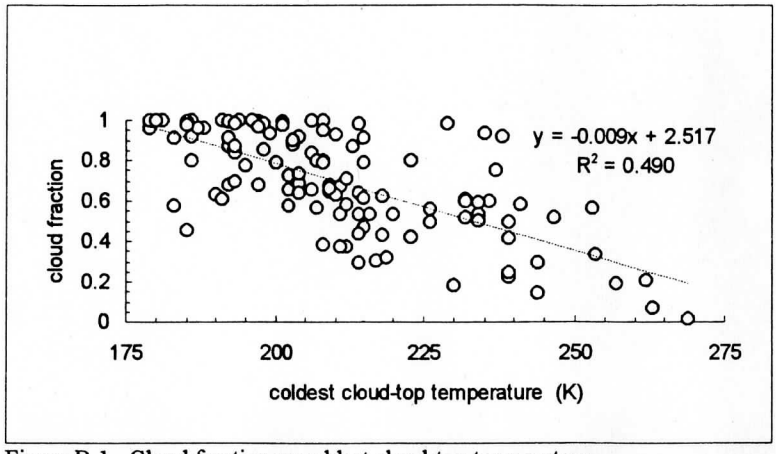

Figure B-1. Cloud fraction *vs* coldest cloud-top temperature.

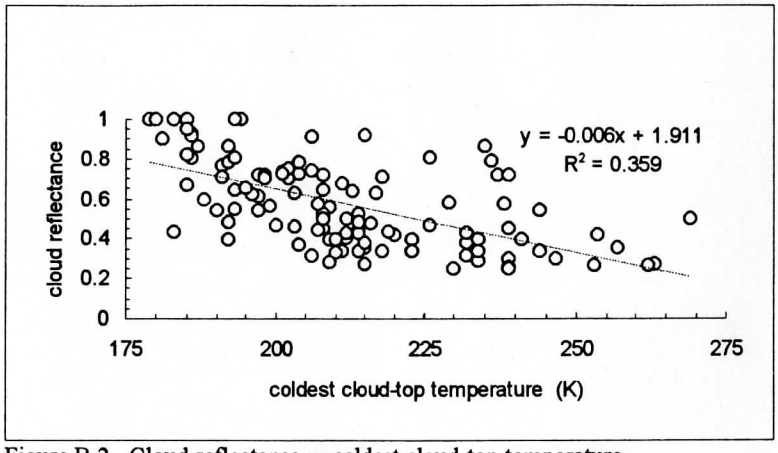

Figure B-2. Cloud reflectance *vs* coldest cloud-top temperature.

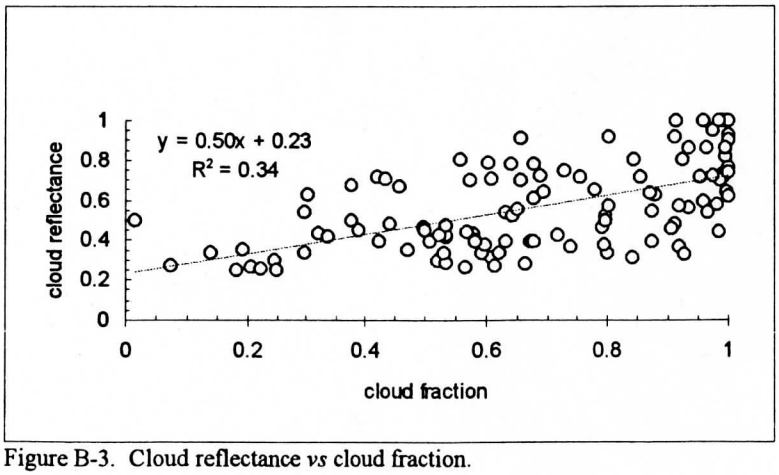

Figure B-3. Cloud reflectance *vs* cloud fraction.

C. Comparisons Between Coldest Top Temperature, Cloud Fraction and Cloud Reflectance

Three figures--one each for minimum cloud-top temperature, cloud fraction and rain class--compare infrared-only and visible/infrared frequencies. A table of frequencies accompanies each figure. In Figures C-1 and C-2 a bin is identified by the value marking the high (warm and cloudy) end of the interval of temperature and cloud fraction, respectively.

Bin	Modc		
	ir only	vis/ir	all
175	0	0	0
180	16	3	19
185	34	7	41
190	48	6	54
195	24	12	36
200	17	8	25
205	21	11	32
210	19	15	34
215	13	16	29
220	14	6	20
225	13	2	15
230	6	4	10
235	5	7	12
240	8	8	16
245	13	3	16
250	8	1	9
255	6	2	8
260	2	1	3
265	0	2	2
270	0	1	1
275	0	0	0

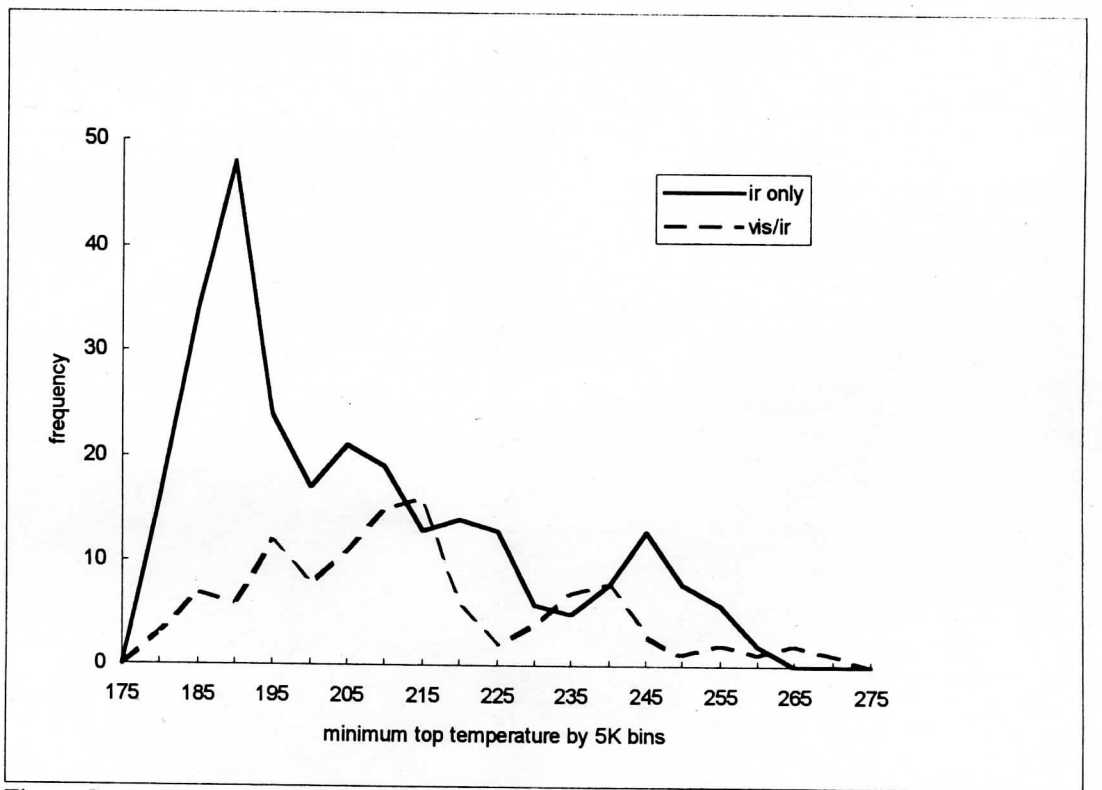

Figure C-1. Infrared-only and visible/infrared frequencies of minimum cloud-top temperature.

Bin	Mode		
	ir only	vis/ir	all
0.05	0	1	1
0.1	0	1	1
0.15	0	1	1
0.2	0	2	2
0.25	0	4	4
0.3	0	2	2
0.35	0	3	3
0.4	0	3	3
0.45	0	4	4
0.5	0	4	4
0.55	0	8	8
0.6	0	9	9
0.65	0	9	9
0.7	0	10	10
0.75	0	3	3
0.8	0	7	7
0.85	0	4	4
0.9	0	5	5
0.95	0	10	10
1	267	25	292

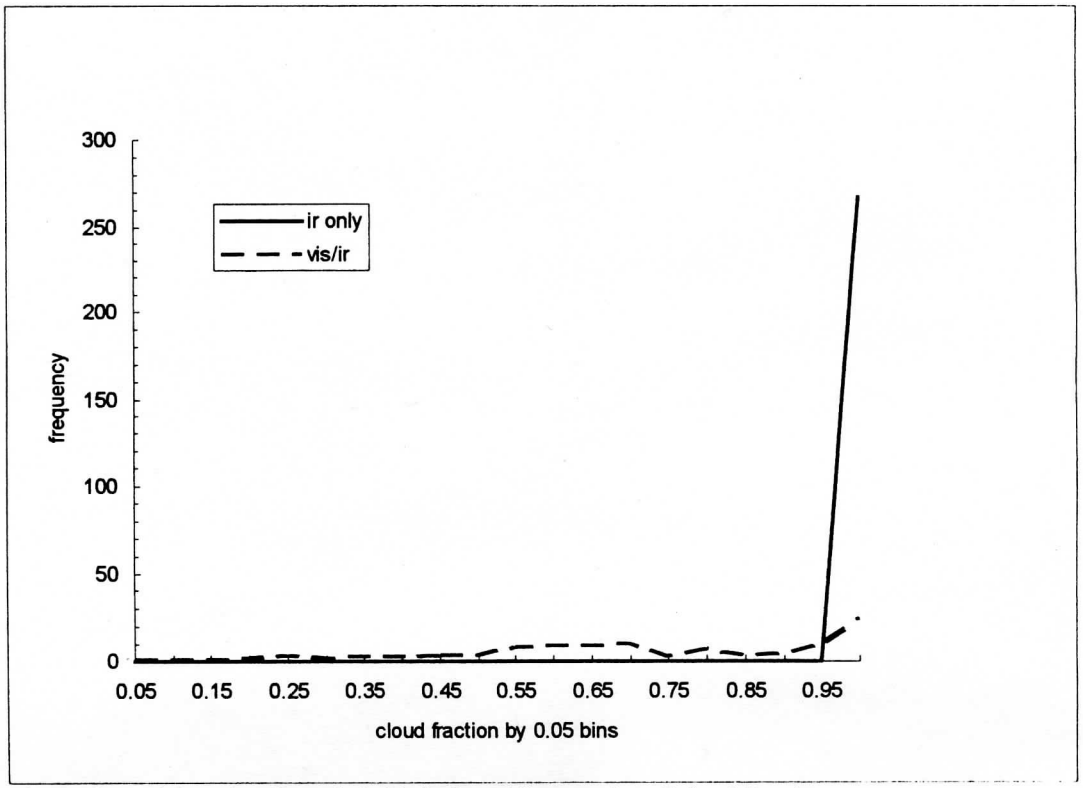

Figure C-2. Infrared-only and visible/infrared frequencies of cloud fraction.

Class	Mode		
	ir only	vis/ir	all
0	13	26	39
1	46	50	96
2	70	33	103
3	23	6	29

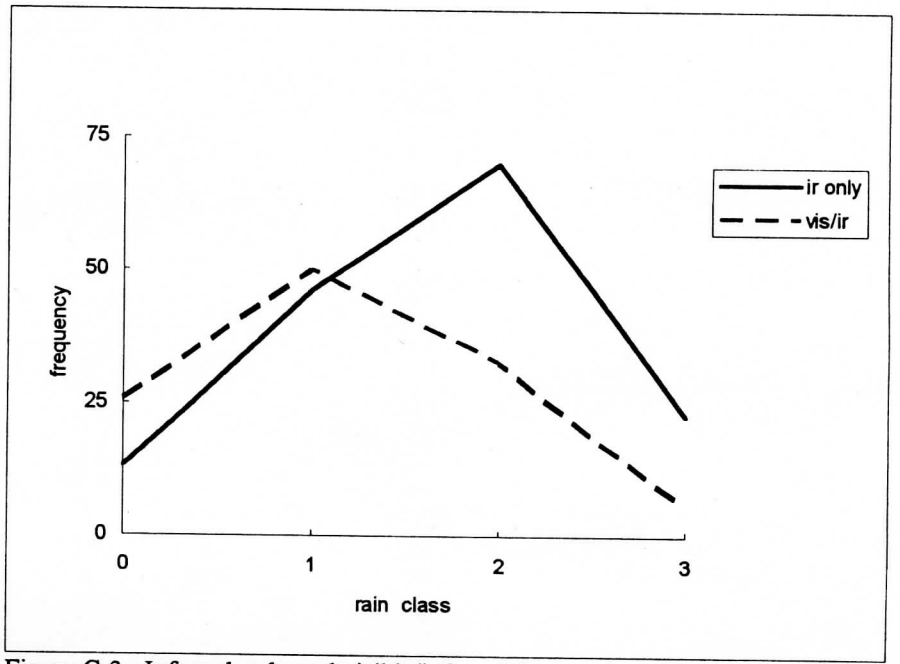

Figure C-3. Infrared-only and visible/infrared frequencies of rain class.